

## Enhanced properties of stone coal-based composite phase change materials for thermal energy storage

Baoshan Xie, Huan Ma, Chuanchang Li, and Jian Chen

Cite this article as:

Baoshan Xie, Huan Ma, Chuanchang Li, and Jian Chen, Enhanced properties of stone coal-based composite phase change materials for thermal energy storage, *Int. J. Miner. Metall. Mater.*, 31(2024), No. 1, pp. 206-215. <https://doi.org/10.1007/s12613-023-2682-x>

View the article online at [SpringerLink](#) or [IJMMM Webpage](#).

### Articles you may be interested in

Xin Wang, Hai Lin, Ying-bo Dong, and Gan-yu Li, [Bioleaching of vanadium from barren stone coal and its effect on the transition of vanadium speciation and mineral phase](#), *Int. J. Miner. Metall. Mater.*, 25(2018), No. 3, pp. 253-261. <https://doi.org/10.1007/s12613-018-1568-9>

Bengisu Yilmaz, Behiye Yüksel, Gökhan Orhan, Devrim Aydin, and Zafer Utlu, [Synthesis and characterization of salt-impregnated anodic aluminum oxide composites for low-grade heat storage](#), *Int. J. Miner. Metall. Mater.*, 27(2020), No. 1, pp. 112-118. <https://doi.org/10.1007/s12613-019-1890-x>

Jun-yi Xiang, Xin Wang, Gui-shang Pei, Qing-yun Huang, and Xue-wei Lü, [Solid-state reaction of a CaO-V<sub>2</sub>O<sub>5</sub> mixture: A fundamental study for the vanadium extraction process](#), *Int. J. Miner. Metall. Mater.*, 28(2021), No. 9, pp. 1462-1468. <https://doi.org/10.1007/s12613-020-2136-7>

Jing Wen, Tao Jiang, Mi Zhou, Hui-yang Gao, Jia-yi Liu, and Xiang-xin Xue, [Roasting and leaching behaviors of vanadium and chromium in calcification roasting-acid leaching of high-chromium vanadium slag](#), *Int. J. Miner. Metall. Mater.*, 25(2018), No. 5, pp. 515-526. <https://doi.org/10.1007/s12613-018-1598-3>

Jing-peng Wang, Yi-min Zhang, Jing Huang, and Tao Liu, [Synergistic effect of microwave irradiation and CaF<sub>2</sub> on vanadium leaching](#), *Int. J. Miner. Metall. Mater.*, 24(2017), No. 2, pp. 156-163. <https://doi.org/10.1007/s12613-017-1390-9>

Majid Hosseini and Mohammad Hossein Paydar, [Fabrication of phosphor bronze/Al two-phase material by recycling phosphor bronze chips using hot extrusion process and investigation of their microstructural and mechanical properties](#), *Int. J. Miner. Metall. Mater.*, 27(2020), No. 6, pp. 809-817. <https://doi.org/10.1007/s12613-020-1980-9>



IJMMM WeChat



QQ author group

# Enhanced properties of stone coal-based composite phase change materials for thermal energy storage

Baoshan Xie<sup>1,2)</sup>, Huan Ma<sup>1)</sup>, Chuanchang Li<sup>1,2),✉</sup>, and Jian Chen<sup>1,2)</sup>

1) Key Laboratory of Renewable Energy Electric-Technology of Hunan Province, School of Energy and Power Engineering, Changsha University of Science and Technology, Changsha 410114, China

2) State Key Laboratory of Disaster Prevention and Reduction for Power Grid, Changsha University of Science and Technology, Changsha 410114, China

(Received: 18 January 2023; revised: 3 May 2023; accepted: 22 May 2023)

**Abstract:** Phase change materials (PCMs) can be incorporated with low-cost minerals to synthesize composites for thermal energy storage in building applications. Stone coal (SC) after vanadium extraction treatment shows potential for secondary utilization in composite preparation. We prepared SC-based composite PCMs with SC as a matrix, stearic acid (SA) as a PCM, and expanded graphite (EG) as an additive. The combined roasting and acid leaching treatment of raw SC was conducted to understand the effect of vanadium extraction on promoting loading capacity. Results showed that the combined treatment of roasting at 900°C and leaching increased the SC loading of the composite by 6.2% by improving the specific surface area. The loading capacity and thermal conductivity of the composite obviously increased by 127% and 48.19%, respectively, due to the contribution of 3wt% EG. These data were supported by the high load of 66.69% and thermal conductivity of 0.59 W·m<sup>-1</sup>·K<sup>-1</sup> of the designed composite. The obtained composite exhibited a phase change temperature of 52.17°C, melting latent heat of 121.5 J·g<sup>-1</sup>, and good chemical compatibility. The SC-based composite has prospects in building applications exploiting the secondary utilization of minerals.

**Keywords:** thermal energy storage; phase change material; stone coal; vanadium extraction; secondary utilization

## 1. Introduction

The “Our World in Data” based on the 2022 BP Statistical Review of World Energy stated that the annual variation in global low-carbon energy generation increased by 5.57% in 2021 [1]. Improving energy utilization efficiency and reducing environmental damage are necessary [2–6] under the pressure of rapid population growth and excessive resource exploitation [7]. Renewable energy, especially solar thermal energy, has attracted increasing attention [8]. However, solar energy utilization has been set back by its disadvantages of unstable and uncontrollable properties [9]. Integrating thermal energy storage (TES) into renewable energy utilization systems is an important way to improve energy efficiency. TES technology is adopted to address the contradictions between heat supply and demand [10–11]. Two types of storage methods based on the mechanism of sensible heat and latent heat are commonly recognized [12]. Latent heat energy storage shows high heat enthalpy and stable phase change temperature when storing/releasing latent heat [13–14]. Therefore, phase change materials (PCMs) are emerging as effective latent heat storage systems and require investigation and application [15–16]. Composite PCMs with good thermal performance must be prepared and applied [17–21].

Stearic acid (SA), which is typical latent heat material, has various advantages as a PCM; these advantages include light weight, nontoxicity, low supercooling, and stability after numerous melting/freezing cycling times [22–25]. Nevertheless, its application is limited by the inherent shortcomings of leakage in the phase change process [26–28]. In view of this limitation, nonmetallic minerals are good choices for incorporation with PCM to prepare composite PCMs and alleviate the disadvantages of pure PCM because of their porous structure and high thermal conductivity. Various minerals, such as kaolinite [29], bentonite [30], palygorskite [31], expanded perlite [32], expanded vermiculite [33], and diatomite [34], commonly serve as matrices in composites [34]. These composites are manufactured into cement boards for buildings or filled into solar thermal storage systems for the application.

The efficient development and utilization of minerals are of great strategic importance for the sustainable supply of resources in China [35]. Stone coal (SC) is a combustible fuel with low carbon content and calorific value [36]. At present, China, especially southern China, has very rich SC reserves. SC has already gained attention due to its relatively low price, absorption capacity, chemical stability, and porous structure. Exploring the use of SC as a matrix to fabricate SC-based composites for building applications is interesting. For example, Li *et al.* [37] compared two types of SCs to study

✉ Corresponding author: Chuanchang Li E-mail: chuanchangli@126.com

© University of Science and Technology Beijing 2024

their mineralogical and thermal storage characteristics. They found that in the melting state, the corresponding SC composites had latent heat values of  $33.02 \text{ J}\cdot\text{g}^{-1}$  and  $29.21 \text{ J}\cdot\text{g}^{-1}$ . Thus far, only a few studies on the utilization of SC to prepare composite PCMs exist. Most researchers choose SC for industrial vanadium extraction [37]. For example, Zeng *et al.* [29] optimized the experimental steps of vanadium extraction and improved the leaching efficiency of vanadium pentoxide through a vanadium extraction experiment. After vanadium extraction, SC was used to prepare composite PCMs; such an approach is a good solution for the secondary utilization of minerals [37]. Importantly, SC after vanadium extraction may affect the structure or surface properties of PCMs. Thus, the thermophysical properties of its corresponding composites must be investigated.

Pure PCM suffers from another disadvantage: low thermal conductivity. The carbon content of SC must be considered to increase the thermal conductivity of composites relative to that of other minerals without carbon. Researchers have added expanded graphite (EG) to composite materials to increase thermal conductivity. For example, Wen *et al.* [38] absorbed PCMs (capric–lauric eutectic acid) by using diatomite to prepare composite PCMs and enhanced thermal conductivity by adding EG. They found that the thermal conductivity of the composite PCMs containing 10wt% EG was improved by 113.2%. Therefore, adding EG to composite PCMs is an effective way to improve performance [34]. Above all, adding EG to SC after vanadium extraction and then loading the resulting material into a PCM is a meaningful attempt at making full use of resources and optimizing composite PCMs.

We attempt to investigate the use of SC in the preparation of composite PCMs with enhanced thermophysical properties by fully exploiting vanadium extraction. Although the treated SC after vanadium extraction can be used as a low-cost raw material for building applications, the effect of analogous vanadium extraction on its properties is unclear. Mineral pretreatment can leverage mineral resources [39]. SC was subjected to combined roasting and acid treatment with sulfuric acid (1.5wt%) to improve its loading capability. EG was added to the composite to improve the thermal conductivity of the treated SC. The designed composite PCMs were manufactured via vacuum impregnation. In addition, the microscopic morphology, thermal stability, and thermal storage characteristics of the SC-based composite PCMs were studied.

## 2. Experimental

### 2.1. Materials

Raw SC with an average size of 200 mesh (0.074 mm) was obtained from Henan, China. SA ( $\text{CH}_3[\text{CH}_2]_{16}\text{COOH}$ ) from Tianjin Hengxing Chemical Regent Co., Ltd., China, was used as the PCM.  $\text{H}_2\text{SO}_4$  solution (analytical reagent, 98%) was purchased from Zhuzhou Xingkonghuabo Co., Ltd., China. EG, with an average size of 300 mesh, was com-

mercially supplied by Qingdao Tengshengda Carbon Co., Ltd. China.

### 2.2. Pretreatment of SC matrix materials

The raw SC was treated through high-temperature roasting and acid leaching. First, 5 g of raw SC was roasted in a muffle stove at  $900^\circ\text{C}$  for 1, 2, and 3 h. Then, the roasted SC was leached in 1.5wt%  $\text{H}_2\text{SO}_4$  solution for 3 h in a 500 mL beaker. The samples were vacuum filtered, washed with distilled water, and dried at  $80^\circ\text{C}$  for 15 h. The obtained SC-based matrix materials treated at  $900^\circ\text{C}$  for different roasting times of 1, 2, and 3 h after leaching were named as SC1L, SC2L, and SC3L, where “L” refers to leaching. Furthermore, the raw SC materials were roasted at different temperatures ( $800$  and  $850^\circ\text{C}$ ) for 2 h before and after acid leaching to investigate the effects of the roasting temperature and acid leaching on the structures (for the detailed analysis of effects, refer to the Supplementary Information).

### 2.3. Preparation of SA/SC and SA/SCs/EG composites

The composite PCMs were prepared through vacuum impregnation [40]. An excessive amount of PCM and an appropriate amount of the matrix were placed in an Erlenmeyer flask that was connected to an antisuction device then to a suction pump. The sample in the Erlenmeyer flask was kept in a vacuum of  $-0.1 \text{ MPa}$  for 5 min, then at  $95^\circ\text{C}$  for 30 min. Next, the samples were cooled to room temperature. Finally, the samples were filtered at  $80^\circ\text{C}$  to remove excess PCM and obtain the final composites. In the preparation process, SA was used as the PCM and the raw and treated SC samples were used as the matrices. The obtained SC-based composites were designated as SA/SC, SA/SC1L, SA/SC2L, and SA/SC3L.

Another type of composite with EG additives was prepared. First, EG and SC1L were mixed together. Then, the mixture was used as the matrix for loading SA through the above-mentioned vacuum impregnation method to prepare composites. The composites with different mixing mass ratios of EG and SC1L ( $\frac{m_{\text{EG}}}{m_{\text{SC1L}}} = 0.05, 0.1, \text{ and } 0.2$ ) were named SA/SC1L/EG<sub>0.05</sub>, SA/SC1L/EG<sub>0.1</sub>, and SA/SC1L/EG<sub>0.2</sub>. Given that EG is an additive and has a very large unit mass volume [34],  $\frac{m_{\text{EG}}}{m_{\text{SC1L}}} = 0.1$  was considered the suitable ratio. The preparation of the matrix materials and composites is illustrated in Fig. 1.

### 2.4. Characterization

X-ray diffraction (XRD) data were collected by using a D8 ADVANCE analyzer (Cu  $K_\alpha$ ) at the voltage of 40 kV and current of 250 mA. The crystalline phases of the composite were analyzed by using the software Jade 6.5. Scanning electron microscopy (SEM) was performed with Zeiss Sigma 500. Fourier transformation infrared spectroscopy (FTIR) spectra were recorded by using an IRtracer-100AH FTIR spectrometer at a voltage of 20 kV. Thermogravimetric analysis (TGA) data were obtained through TGA-differential

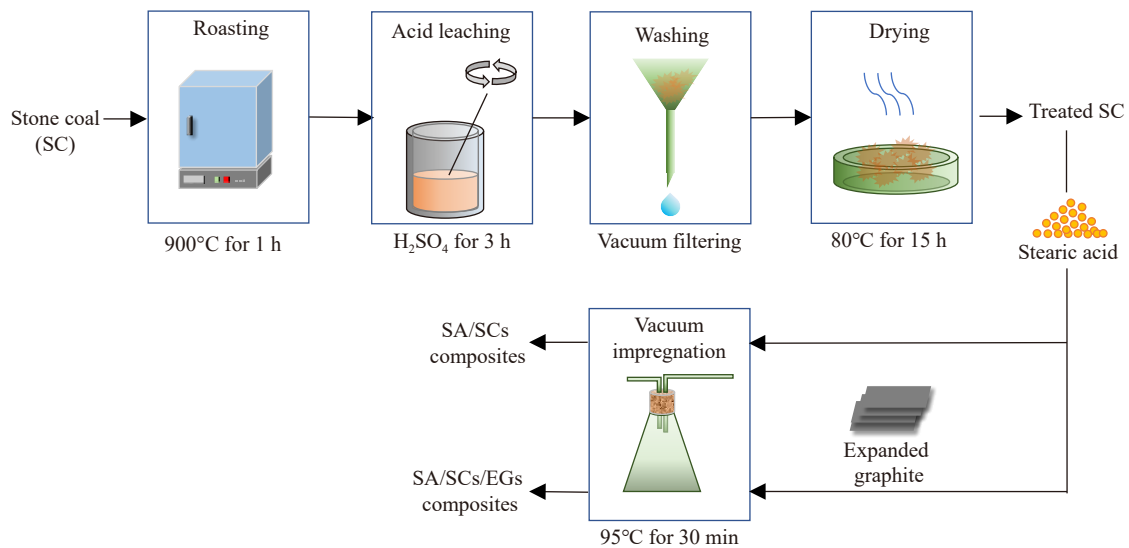


Fig. 1. Preparation of SC matrix materials and SA/SC and SA/SCs/EG composites.

scanning calorimetry (DSC) with the HCT-3 model from Beijing Henven Scientific Instrument Factory, China, at a heating rate of  $15^{\circ}\text{C}\cdot\text{min}^{-1}$  in a nitrogen atmosphere. DRX-I-300 was used to record the thermal conductivity of the samples, which were pressed into plate tablets with a thickness of approximately 1 mm and a diameter of 12 mm. A tablet was placed between a compressive load and another support load composed of copper. Heat flux through the tablet sample was recorded during testing. DSC was performed with TA Instruments DSC Q10 (V9.9 Build 303) at a heating rate of  $5^{\circ}\text{C}\cdot\text{min}^{-1}$  in an argon atmosphere. Liquid nitrogen was used to cool the sample during the freezing period. The thermal storage and release performances of SA and composite PCMs were studied by using experimental equipment with a thermocouple accuracy of  $0.1^{\circ}\text{C}$ . The nitrogen gas absorption–desorption isotherms of the matrix were obtained by using ASAP 2020 with an accuracy of 2%. Thermal infrared images were acquired by using FLUKE Ti450 with a noise equivalent temperature difference of  $0.05^{\circ}\text{C}$ . Samples were pressed into round sheets approximately 1.8 mm thick and placed on a heat/cold source for heating/cooling. The temperature of the sample was recorded by using a thermal infrared camera. The heat storage/release test in this work was conducted by using a lab-made device with a thermostat water

bath, wherein thermocouples were inserted inside the sample to record temperature variation. This method was introduced in a previous work [41].

### 3. Results and discussion

#### 3.1. Crystallization structure

The XRD patterns of the matrix materials and composites are shown in Fig. 2. Comparison among the EG, SC, SC1L, and SC1L/EG<sub>0.1</sub> matrices (Fig. 2(a)) reveals that EG presents two strong graphite peaks of the regular crystallization (002) plane at  $2\theta = 27.0^{\circ}$  and the (004) plane at  $2\theta = 55.8^{\circ}$ . The raw SC shows two obvious peaks in the range of  $2\theta = 20^{\circ}$ – $30^{\circ}$ . Both peaks are the characteristic peaks of quartz ( $2\theta = 20.8^{\circ}$  for (100) plane and  $2\theta = 26.6^{\circ}$  for (101) plane). Notably, SC1L and the SC matrix have similar XRD patterns. Moreover, the XRD patterns of raw SC at different roasting temperatures and times and before/after acid leaching (Fig. S1) demonstrate that roasting and acid leaching have little effect on the crystal structure of SC. The physical mixture of SC1L/EG<sub>0.1</sub> only shows two peaks because the characteristic peaks of EG and SC at approximately  $2\theta = 27^{\circ}$  formed an overlapping peak due to their closeness. This result accounts for the larger width of the overlapping peak than

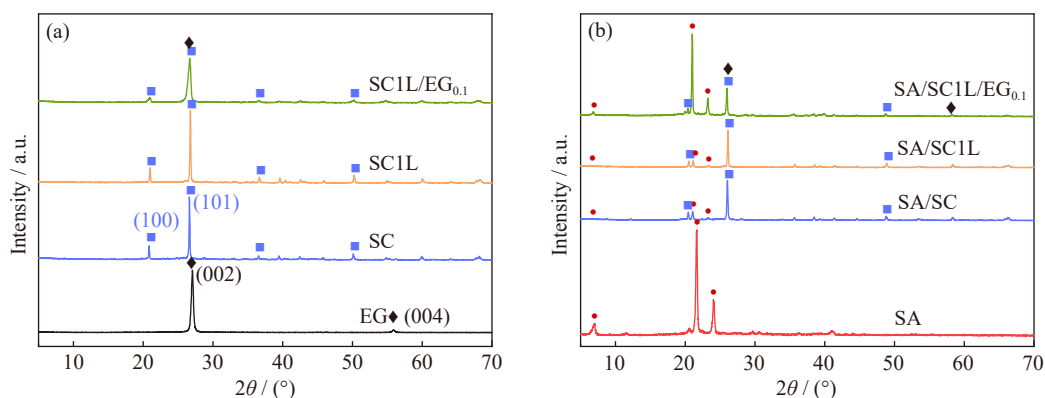


Fig. 2. XRD patterns of (a) matrix materials and (b) pure SA and composites.

that of the single peak in EG or SC. Fig. 2(b) shows the comparison of pure SA and the SA/SC, SA/SC1L, and SA/SC1L/EG<sub>0.1</sub> composites. In this figure, SA presents a strong peak at approximately  $2\theta = 21.6^\circ$  and  $24.0^\circ$ . The SC-based composite materials contain all characteristic peaks from pure SA and matrix materials. Although no additional peaks have appeared, peak strength differs. The intensities of the characteristic peak of SA in the composites differ due to the diverse SA contents. SA/SC1L/EG<sub>0.1</sub> thus has the strongest peak.

### 3.2. Chemical structure and compatibility

The FTIR curves of the tested materials are presented in Fig. 3. In the spectrum of SC (Fig. 3(a)), the band at  $469\text{ cm}^{-1}$  is attributed to the bending of Si–O and Si–O–Si [42], that at  $515\text{ cm}^{-1}$  is due to Si–O–Al<sup>VI</sup> [29], and that at  $694\text{ cm}^{-1}$  is the stretching vibration of Si–O–Si [37]. The bands at 797 and  $1088\text{ cm}^{-1}$  are the symmetric stretching vibration of Si–O–Si in quartz and the antisymmetric stretching vibration of Si–O–Si [37]. The absorption at  $3427\text{ cm}^{-1}$  originates from loosely bound water ( $\nu[\text{H–O–H}]$ ) [22]. The FTIR spectra at

$1088\text{ cm}^{-1}$  of SC (Fig. S2) and SC1L are more intense than those of SC because roasting and acid leaching remove unstable structures and impurities from SC. The peaks at  $1088$  and  $3427\text{ cm}^{-1}$  in SC after roasting and acid leaching have widened because roasting and acid leaching destroyed the silica tetrahedral structure of SC and removed moisture from most of the structures in SC, as illustrated in Fig. S2. In the SA spectrum (Fig. 3(b)), the bands at  $2916$  and  $2850\text{ cm}^{-1}$  are attributed to the asymmetric and symmetrical stretching vibration peaks of  $-\text{CH}_2$ , respectively. The band at  $1705\text{ cm}^{-1}$  is due to the C=O stretching of carboxylic groups. The band at  $1472$  and  $1310\text{ cm}^{-1}$  originated from the in-plane bending vibration peak of OH groups. The band at  $718\text{ cm}^{-1}$  is due to the in-plane swinging vibration peak of  $-\text{OH}$  groups [43–45]. The spectrum of SC-based composite PCMs containing the matrix materials and SA is also presented in Fig. 3(b). The spectrum indicates that SA and the matrix materials do not undergo chemical interaction during composite preparation given that it contains no obvious new characteristic peaks. Therefore, the preparation of the composites only has physical effects.

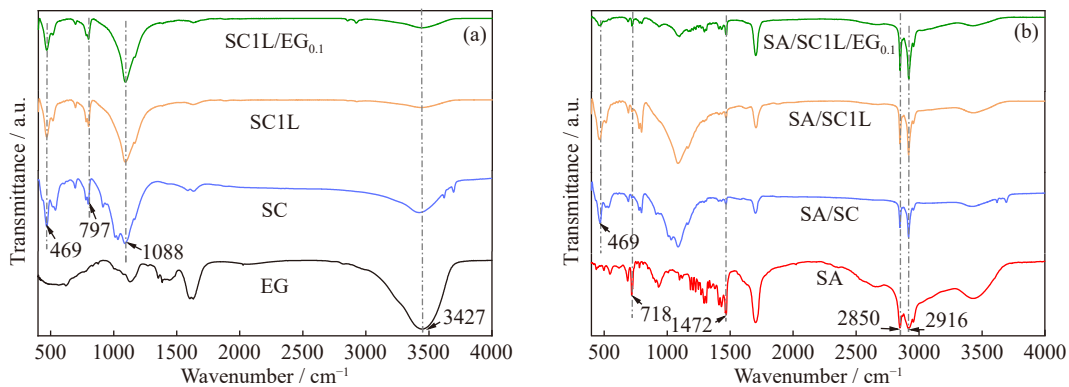


Fig. 3. FTIR curves of (a) matrices and (b) SA and SC-based composites.

### 3.3. Morphology and microstructures

The SEM images of SC, SC matrix after roasted at  $900^\circ\text{C}$  for 1 h, SC1L, SC1L/EG<sub>0.1</sub>, and their corresponding composites are provided in Fig. 4. The raw SC (Fig. 4(a)) contains small, flake-shaped particles that are mainly derived from layered quartz and aluminosilicate minerals as proven by XRD analysis. SC roasted at  $900^\circ\text{C}$  for 1 h (Fig. 4(b)) appears to be purified, given that the flake-like particles are easily observed because impurities have been removed. After acid leaching, the SC1L matrix (Fig. 4(c)) shows rod-like minerals, indicating that the matrix has been purified due to the erosion of additional pores by acid leaching. In other words, acid leaching can cause slight structural damage to raw SC to increase the pore space, resulting in a higher PCM loading of SC1L than that of SC. The effect of roasting and acid leaching on the obtained vanadium ion leaching rate is presented in Table S1. In the images of the SA/SC1L composite (Fig. 4(d)), SA has completely covered the surface of SC1L after impregnation, and SA has been successfully loaded into the small pores of SC1L. Moreover, the images of

the SC1L/EG<sub>0.1</sub> matrix in Fig. 4(e) show that although SC1L and EG have mixed together, they have not reacted with each other, and part of the SC1L particles are dispersed inside EG. The SA/SC1L/EG<sub>0.1</sub> composite (Fig. 4(f)) shows that the mixture of EG and SC1L is covered by SA but is not uniform because the matrix materials in the mixture have different particle sizes. Thus, the addition of EG does not affect the composite PCM loaded with SA [34].

The pore structure and Balanced-Emitter Transistor (BET) surface areas of the materials were analyzed through the nitrogen adsorption/desorption method. The  $\text{N}_2$  adsorption/desorption isotherms are shown in Fig. 4(g) and (h). Both samples have a type-III isotherm with a hysteresis loop at a relative pressure ( $P/P_0 > 0.6$ ), reflecting the existence of mesopores and macropores in matrix materials. Fig. 4(i) shows the pore size and volume distribution. Although the pore size distributions of SC and SC1L have similar trends, SC1L has slightly larger micropore ( $<5\text{ nm}$ ) and macropore ( $>50\text{ nm}$ ) volumes than SC. The detailed analysis of pore properties is introduced in Fig. S3(a)–(d). The adsorption/desorption curves of the pore properties of the SC and SC1L

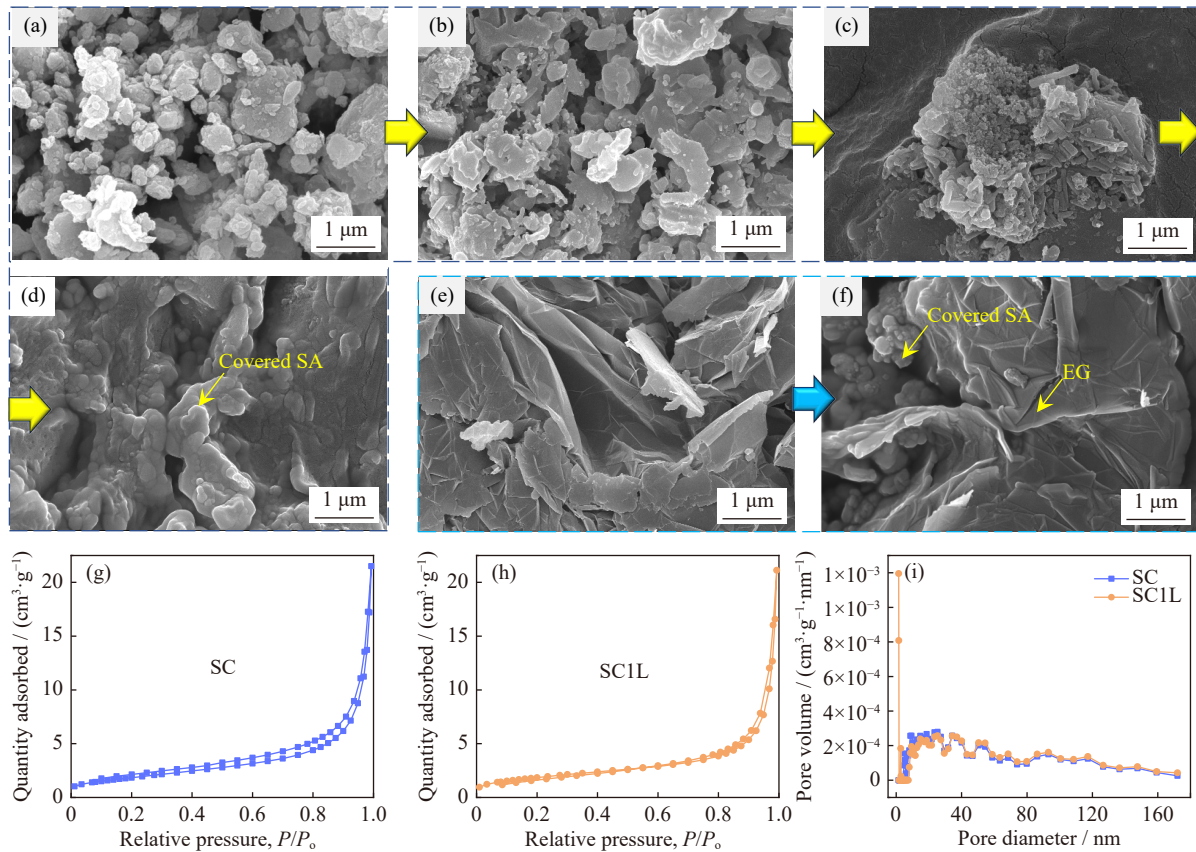


Fig. 4. SEM images: (a) SC matrix, (b) SC matrix after roasted at 900°C for 1 h, (c) SC1L matrix, (d) SA/SC1L composite, (e) SC1L/EG<sub>0.1</sub> matrix, and (f) SA/SC1L/EG<sub>0.1</sub> composite; BET analysis: (g) adsorption/desorption curve of SC, (h) adsorption-desorption curve of SC1L, and (i) pore diameter distribution of SC and SC1L.

samples show that the BET-specific surface area of SC1L ( $6.8671 \text{ m}^2 \cdot \text{g}^{-1}$ ) is larger than that of SC ( $6.8366 \text{ m}^2 \cdot \text{g}^{-1}$ ). This finding is indicative of a large specific surface area that can provide additional adsorption sites for PCM. The Barret-Joyner-Halenda (BJH) adsorption average pore diameter of SC1L (21.34 nm) is also larger than that of SC (19.36 nm). Therefore, comparing the SC and SC1L samples shows that the combined roasting and acid leaching treatment can influence pore properties.

### 3.4. Thermal stability and loading capability

We further investigated the decomposition of composites by using the TGA method (Fig. 5). As presented in Fig. 5(a) and (c), all composite samples exhibit negligible mass loss at 200°C. This result highlights the good thermal stability of the samples. Only SA/SC shows slight weight loss at 100°C owing to the absorbed water in its matrix. Increasing the decomposition temperature from 200 to 750°C results in similar curves of the composites, except for that of the SA/SC composite, and no new mass loss stage is observed. The decomposition of SA leads to a single degradation process of SC-based composites between 200–300°C. The corresponding DSC curves (Fig. 5(b) and (d)) also verify that an endothermic peak exists at approximately 200–300°C, indicating that SA has been degraded [46]. However, at temperatures beyond 500°C, only the SA/SC composite loses weight due to the dehydration of lattice water in raw SC [37]. Therefore,

the treated SC shows improved stability after roasting and acid leaching. The composites using SC as the matrix have higher thermal stability than the basic SA/SC.

The TGA curve can be used to calculate the SA loading capacity of the SC-based PCM. Loadage ( $\delta$ , %) is defined as the mass ratio of PCM to the total composite, as shown below:

$$\delta = \frac{m_{\text{PCM}}}{m_{\text{matrix}} + m_{\text{PCM}}} \times 100\% \quad (1)$$

where  $m_{\text{PCM}}$  (g) is the mass of pure PCM, and  $m_{\text{matrix}}$  (g) represents the mass of the matrix.

Therefore, the  $\delta$  values of SA in SA/SC, SA/SC1L, SA/SC2L, and SA/SC3L are 18.50%, 24.71%, 23.62%, and 21.60%, respectively (Fig. 5(a)). SA/SC1L has the highest PCM loadage. Roasting and acid leaching can increase the loading capacity of the raw SC matrix by increasing pore space, as proven by BET analysis. However, the composite prepared with the other two matrices and a long roasting time does not show increased loading. The slight reduction in loading is due to the long roasting time. The macropore structure is damaged such that constraining PCM is difficult, as supported by the leaching rate of vanadium ions shown in Table S1. The  $\delta$  values of SA in the three SA/SC1L/EG composites with  $\frac{m_{\text{EG}}}{m_{\text{SC1L}}} = 0.05, 0.1, \text{ and } 0.2$  are 52.65%, 66.69%, and 78.59%, respectively. EG has a considerable pore space that increases with the increase in the proportion of EG and

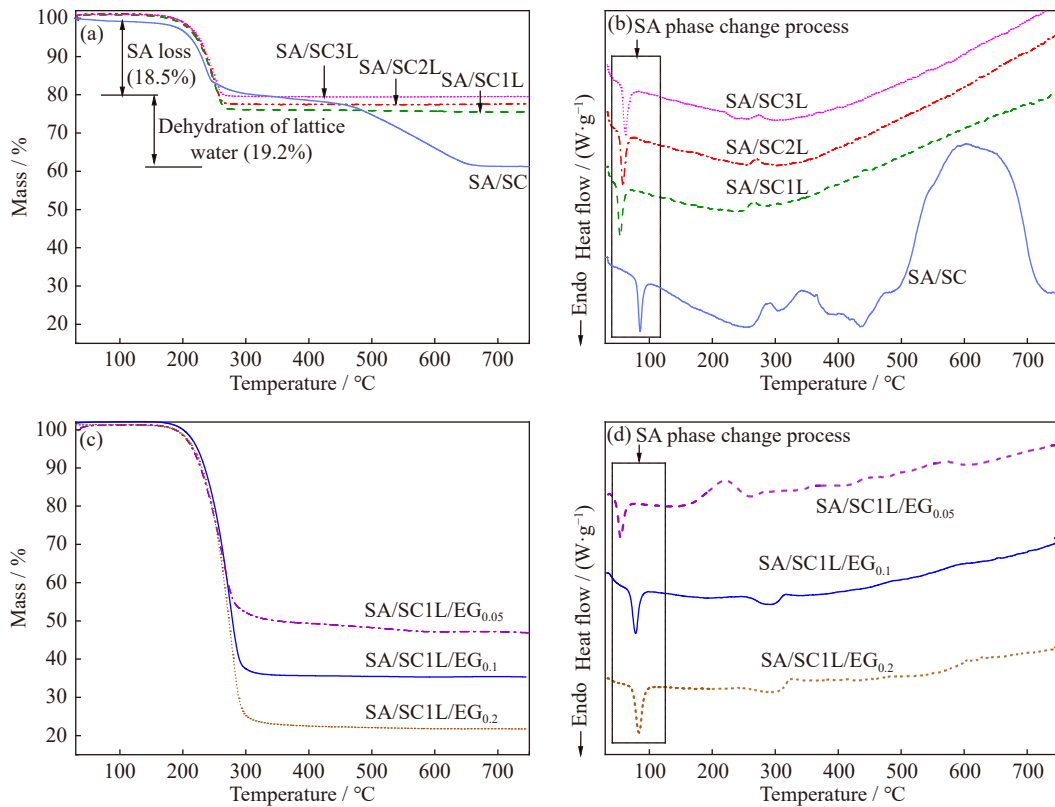


Fig. 5. (a, c) TGA and (b, d) TG-DSC curves of the SC-based composites.

the loading of SA. Above all, the results show that the combined roasting and acid leaching treatment increases the loading capacity of SC by 6.2% by increasing the specific surface area. However, prolonging the roasting time will not improve the loading capacity continuously. The addition of EG<sub>0.1</sub> has improved the loading capacity of the prepared SA/SC1L/EG<sub>0.1</sub> composite by 48.19% relative to that of SA/SC.

### 3.5. Phase change behavior and enthalpy

The DSC curves of the SC-based composite PCMs and SA are presented in Fig. 6. The curves in Fig. 6(a) and (b) present obviously similar shapes but dissimilar areas, indicating comparable phase change behavior. Table 1 lists the corresponding thermal properties of the samples. SA, as a pure PCM, melts at approximately 52.91°C. The melting phase transition temperatures of SA/SCs are 52.81–52.93°C, and those of SA/SCs/EGs are 52.17–52.41°C. The phase transition point of the composite PCMs during melting differs by

1°C and is slightly affected by incorporation.

An insignificant difference is found between the latent heat values of one sample in the melting and freezing states. The latent heat of pure SA in the melting state is 191.5 J·g<sup>-1</sup>, and that of pure SA in the freezing state is 190.2 J·g<sup>-1</sup>. Accordingly, the latent heat values of the composites SA/SC, SA/SC1L, SA/SC2L, and SA/SC3L are 33.02, 41.73, 40.97, and 39.32 J·g<sup>-1</sup>, respectively, in the melting state and are 33.17, 41.45, 40.19, and 39.22 J·g<sup>-1</sup>, respectively, in the freezing state. This finding indicates that whether in the melting or freezing state, SA/SC1L has a slightly higher latent heat than the other composites in accordance with its large loading capacity. The latent heat values of the SA/SC1L/EG<sub>0.1</sub>, SA/SC1L/EG<sub>0.05</sub>, and SA/SC1L/EG<sub>0.2</sub> composites are 117.61, 97.11, and 135.2 J·g<sup>-1</sup>, respectively. In the freezing state, the latent heat values of SA/SC1L/EG<sub>0.1</sub>, SA/SC1L/EG<sub>0.05</sub>, and SA/SC1L/EG<sub>0.2</sub> are 118.40, 98.81, and 135.0 J·g<sup>-1</sup>. From the perspective of the latent heat values in

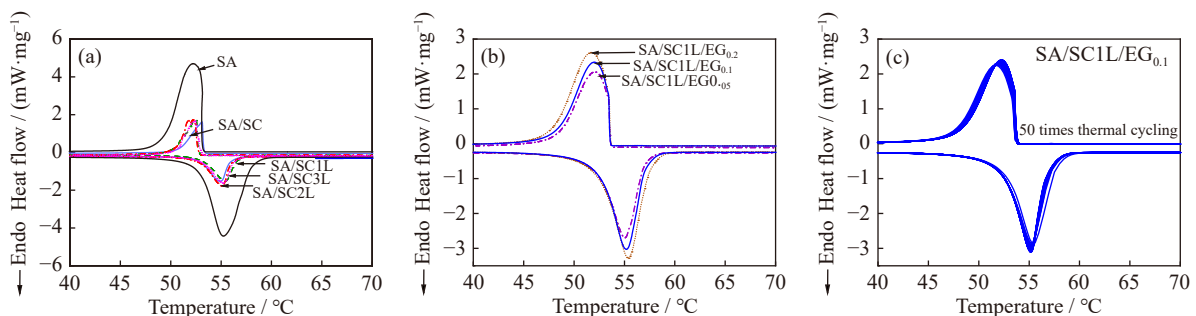


Fig. 6. DSC curves of (a) SA and the SA/SC composites, (b) the SA/SCs/EG composites, and (c) the SA/SC1L/EG<sub>0.1</sub> composite after 50 thermal cycles.

**Table 1. Thermal properties of pure SA and the SC-based composites**

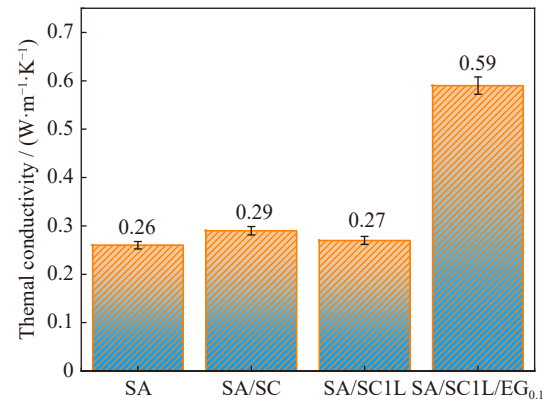
Sample	Loadage, $\beta / \%$	Melting temperature, $T_m / ^\circ\text{C}$	Freezing temperature, $T_f / ^\circ\text{C}$	Latent heat of melting, $\Delta H_m / (\text{J}\cdot\text{g}^{-1})$	Latent heat of freezing, $\Delta H_f / (\text{J}\cdot\text{g}^{-1})$
SA	100	52.91	53.10	191.5	190.2
SA/SC	18.50	52.81	53.24	33.02	33.17
SA/SC1L	24.71	52.93	52.85	42.76	41.32
SA/SC2L	23.62	52.87	52.65	46.87	46.09
SA/SC3L	21.60	52.93	52.95	42.58	42.05
SA/SC1L/EG <sub>0.05</sub>	52.65	52.24	53.58	105.9	103.9
SA/SC1L/EG <sub>0.1</sub>	66.69	52.17	53.54	121.5	119.3
SA/SC1L/EG <sub>0.2</sub>	78.69	52.41	53.60	143.6	142.5

the melting and freezing stages, the latent heat value increases as the added amount of EG increases. As the added amount of EG increases, the thermal storage capacity of the composite increases because EG increases the SA loading of the sample. This behavior shows that SA/SC1L/EG<sub>0.1</sub> has a suitable phase change transition temperature and excellent thermal characteristics.

Composite PCMs must have long-term thermal cycle stability in practical applications. We conducted 50 thermal cycle tests to evaluate the reliability of the SA/SC1L/EG<sub>0.1</sub> composite PCM. Fig. 6(c) shows that its latent heat values have slight changes and that its phase transition temperature does not change significantly. After 50 cycles, the phase change temperatures of the sample in the melting and freezing states have increased by 0.25°C and 0.07°C, respectively. The latent heat values of the sample in the melting and freezing states have decreased by 0.44% and 1.02%, respectively, and tend to be stable. In summary, the tested composite PCMs can be recycled without performance degradation.

### 3.6. Thermal conductivity

The thermal conductivity of the SC-based composite PCMs and pure SA are shown in Fig. 7. The SA/SC, SA/SC1L, and SA/SC1L/EG<sub>0.1</sub> composites have higher thermal conductivities of 0.29, 0.27, and 0.59 W·m<sup>-1</sup>·K<sup>-1</sup>, respectively, than pure SA, which has a thermal conductivity of 0.26 W·m<sup>-1</sup>·K<sup>-1</sup>. This result reflects that the matrix present in the composite can increase the thermal conductivity of PCMs. Among the composites shown in the figure, SA/SC1L/EG<sub>0.1</sub> has the highest thermal conductivity. The thermal conductivity of SA/SC1L/EG<sub>0.1</sub> has increased by 127% relative to that of pure SA because adding EG to the composite increases heat transfer pathways [46], even though

**Fig. 7. Thermal conductivities of SA and composites.**

the TGA results show that the corresponding composite has the lowest matrix content. For example, although the mass fraction of the SC1L/EG matrix in the SA/SC1L/EG<sub>0.1</sub> composite is 33.31wt%, the addition of only 3.03wt% EG can significantly enhance the thermal conductivity of SA/SC1L/EG<sub>0.1</sub>. Table 2 exhibits the comparison of the thermophysical properties of the SA/SC1L/EG<sub>0.1</sub> composite with those of other composites in the literature [47–50]. SA/SC1L/EG<sub>0.1</sub> has better thermal performance, such as higher thermal conductivity, appropriate melting temperature, and considerable latent heat capacities, than the reported composites.

### 3.7. TES/release behavior

We evaluated the TES/release performance of SA, SA/SC, and SA/SC1L/EG<sub>0.1</sub> by heating/cooling the samples in a self-designed device. First, samples with the same initial temperature were placed in a water bath at 80°C for heating. After their temperature had stabilized, the samples were moved to a

**Table 2. Comparison of the thermophysical properties of the prepared SA/SC1L/EG<sub>0.1</sub> composite with those of other composites in the literature**

Samples	Melting temperature, $T_m / ^\circ\text{C}$	Freezing temperature, $T_f / ^\circ\text{C}$	Latent heat of melting, $\Delta H_m / (\text{J}\cdot\text{g}^{-1})$	Latent heat of freezing, $\Delta H_f / (\text{J}\cdot\text{g}^{-1})$	Thermal conductivity / (W·m <sup>-1</sup> ·K <sup>-1</sup> )	Ref.
Myristate/diatomite/EG	45.86	44.63	96.21	92.46	0.22	[47]
Lauric acid/expanded perlite/EG	43.80	40.20	86.70	86.90	0.13	[48]
Paraffin/calcined diatomite	33.04	52.43	89.54	89.80	—	[49]
Capric acid/expanded perlite/EG	31.60	31.50	96.30	—	0.14	[50]
SA/SC1L/EG <sub>0.1</sub>	52.17	53.54	117.61	118.4	0.59	This work

cold source with a temperature of 20°C for cooling. The temperature–time curves for heating and cooling were recorded and are shown in Fig. 8. A single curve has three stages representing different temperature variation rates. Each stage refers to the sensible, latent, and sensible heat storage process. The abrupt change in the rate of temperature variation in the curves is related to the phase change point because PCM stores/releases heat within a narrow range of phase change temperatures. However, in practice, the beginning and end

points of the latent heat storage process are slightly different, accounting for the observed nonhorizontal phase change stage platform. Qualitatively, the temperature variation rate during the heat storage/release process is mainly affected by the thermal conductivity of the sample. The high thermal conductivity of SA/SC1L/EG<sub>0.1</sub> is indicative of a high temperature variation rate such that additional energy is stored/released within the same time under the same boundary condition.

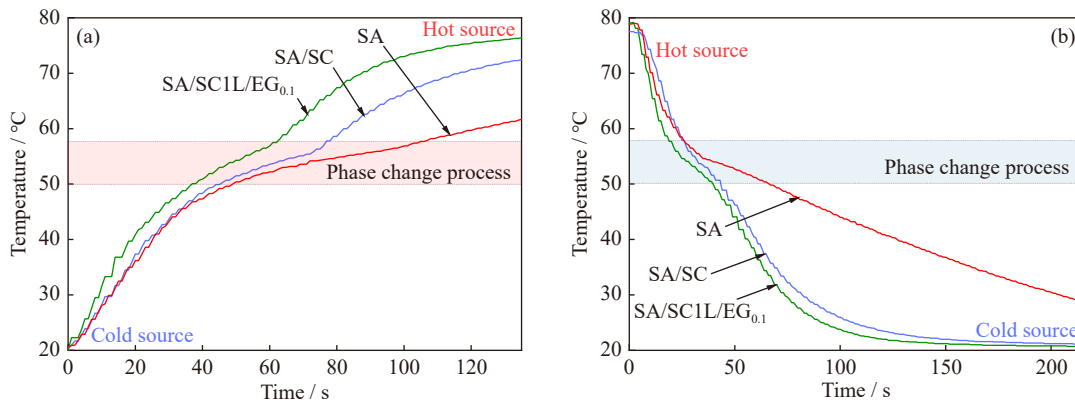


Fig. 8. Temperature–time curves of the pure SA and composites during (a) storage and (b) release.

SA/SC1L/EG<sub>0.1</sub> presents the steepest curve among the three samples during heating (Fig. 8(a)) mainly because it has the highest thermal conductivity. The thermal storage curves show that SA takes 52 s, and the composites (SA/SC and SA/SC1L/EG<sub>0.1</sub>) with high thermal conductivity take only 47 and 38 s to reach 50°C from an initial temperature of approximately 20°C. The thermal release curves demonstrate that during cooling (Fig. 8(b)), SA takes 34 s, and the SA/SC and SA/SC1L/EG<sub>0.1</sub> composites take 30 and 25 s, respectively, to reach 55°C from the initial temperature of approximately 78°C. This finding illustrates that the heat storage ability of composite materials is better than that of SA. Studying the

thermal storage and thermal release abilities of the composite PCMs and SA proves that the addition of EG enhances the performance of the composite PCMs.

The thermal response behaviors of SA/SC1L and SA/SC1L/EG<sub>0.1</sub> were recorded by using a thermal infrared camera, as shown in Fig. 9. In the infrared images, the change in color from black to red represents increases in temperature (Fig. 9(a)). During heating, the temperature of SA/SC1L/EG<sub>0.1</sub> takes 43 s to increase to 55°C from an initial value of 28°C. During this process, the temperature variation rate of SA/SC1L is lower than that of SA/SC1L/EG<sub>0.1</sub>, although the temperatures of both samples are increasing. The same situ-

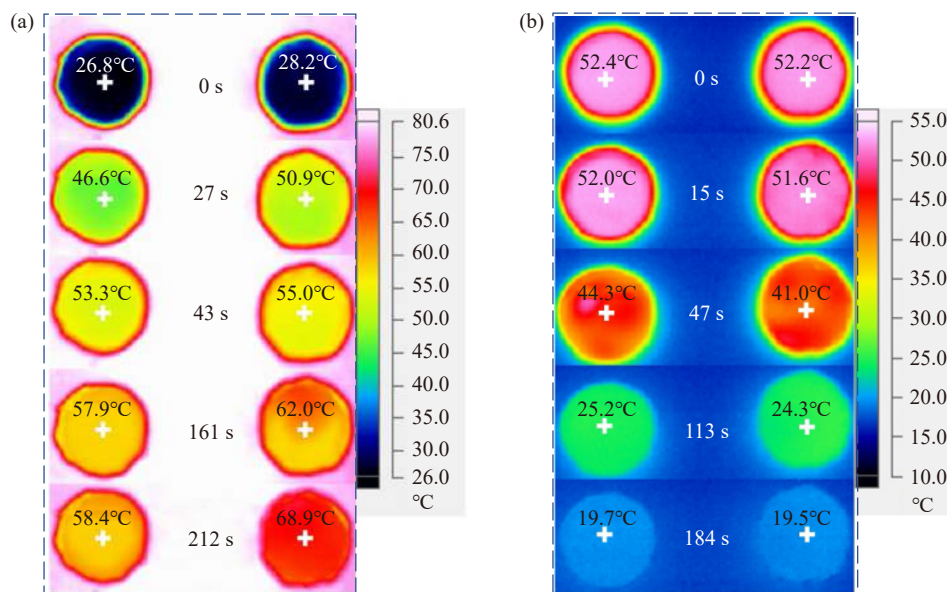


Fig. 9. Thermal infrared images of SA/SC1L (left) and SA/SC1L/EG<sub>0.1</sub> (right) during (a) heating and (b) cooling.

ation occurs when the samples are cooled from 52°C to the ambient temperature, and the cooling rate of SA/SC1L/EG<sub>0.1</sub> is faster than that of SA/SC1L (Fig. 9(b)). This finding suggests that the response rate of SA/SC1L is lower than that of SA/SC1L/EG<sub>0.1</sub> at the same external temperature. SA/SC1L/EG<sub>0.1</sub> has a great advantage over SA/SC1L in terms of transient temperature response.

#### 4. Conclusions

SC-based composite PCMs were prepared by loading SA into an SC-based matrix. Their microstructures, morphologies, thermophysical properties, and phase change behaviors were investigated by using different characterization techniques and a self-designed device. Our main conclusions are summarized as follows.

(1) The combined treatment of roasting at 900°C for 1 h and acid leaching increased the SC loadage of the composites by 6.2% by enlarging the specific surface areas of pores.

(2) The loadage of the SC-based composites (SA/SC1L/EG<sub>0.1</sub>, 66.69%) added with EG improved by 48.19% relative to that of the composites without EG (SA/SC1L, 18.50%). No chemical reaction occurred between the SC matrix and SA during the preparation of the composites.

(3) The thermal conductivity of the prepared SA/SC1L/EG<sub>0.1</sub> composite is 127% (0.59 W·m<sup>-1</sup>·K<sup>-1</sup>) higher than that of pure SA, indicating that the transient temperature response behavior of this composite had improved. The phase change temperature and melting latent heat of the composite were 52.17°C and 121.5 J·g<sup>-1</sup>, respectively.

(4) All composites adopting the treated SC matrix showed good thermal stability at 200°C. However, SA/SC with the raw SC matrix lost absorbed water from its matrix at 100°C and experienced lattice water dehydration at 500–600°C during roasting. These effects worsened its stability.

Overall, SC-based composites can be considered promising PCMs for the full exploitation of SC resources because of their excellent thermal properties, including appropriate melting temperature, use of SC extracted from vanadium, and high thermal conductivity.

#### Acknowledgements

This work was financially supported by the National Natural Science Foundation of China, China (Nos. 52274252 and 51874047), the Special Fund for the Construction of Innovative Provinces in Hunan Province, China (No. 2020RC3038), and the Changsha City Fund for Distinguished and Innovative Young Scholars, China (No. kq1802007).

#### Conflict of Interest

Chuanchang Li is a youth editorial board member for this journal and was not involved in the editorial review or the decision to publish this article. All authors declare that there are

no competing interests.

#### Supplementary Information

The online version contains supplementary material available at <https://doi.org/10.1007/s12613-023-2682-x>.

#### References

- [1] Our World in Data, 2021 Annual Percentage Change in Low-Carbon Energy Generation [2022-01-05]. <https://our-worldindata.org/grapher/annual-percentage-change-low-carbon>.
- [2] C.C. Li, M.F. Wang, Z.S. Chen, and J. Chen, Enhanced thermal conductivity and photo-to-thermal performance of diatomite-based composite phase change materials for thermal energy storage, *J. Energy Storage*, 34(2021), art. No. 102171.
- [3] B. Xiang, X.L. Cao, Y.P. Yuan, *et al.*, A novel hybrid energy system combined with solar-road and soil-regenerator: Sensitivity analysis and optimization, *Renewable Energy*, 129(2018), p. 419.
- [4] X.J. Yang, L.L. Sun, Y.P. Yuan, X.D. Zhao, and X.L. Cao, Experimental investigation on performance comparison of PV/T-PCM system and PV/T system, *Renewable Energy*, 119(2018), p. 152.
- [5] T.T. Wang, C.P. Li, X.S. Xie, *et al.*, Anode materials for aqueous zinc ion batteries: Mechanisms, properties, and perspectives, *ACS Nano*, 14(2020), No. 12, p. 16321.
- [6] A.D. Kamble, V.K. Saxena, P.D. Chavan, and V.A. Mendhe, Co-gasification of coal and biomass an emerging clean energy technology: Status and prospects of development in Indian context, *Int. J. Min. Sci. Technol.*, 29(2019), No. 2, p. 171.
- [7] B. Yilmaz, B. Yüksel, G. Orhan, D. Aydin, and Z. Utlu, Synthesis and characterization of salt-impregnated anodic aluminum oxide composites for low-grade heat storage, *Int. J. Miner. Metall. Mater.*, 27(2020), No. 1, p. 112.
- [8] R.M. Wang, Z.Y. Gao, W.R. Wang, Y. Xue, and D.Y. Fu, Dynamic characteristics of the planetary gear train excited by time-varying meshing stiffness in the wind turbine, *Int. J. Miner. Metall. Mater.*, 25(2018), No. 9, p. 1104.
- [9] K.S. Reddy, V. Mudgal, and T.K. Mallick, Review of latent heat thermal energy storage for improved material stability and effective load management, *J. Energy Storage*, 15(2018), p. 205.
- [10] X.B. Zhao, C.C. Li, K.H. Bai, B.S. Xie, J. Chen, and Q.X. Liu, Multiple structure graphite stabilized stearic acid as composite phase change materials for thermal energy storage, *Int. J. Min. Sci. Technol.*, 32(2022), No. 6, p. 1419.
- [11] C.C. Tseng, R.L. Sikorski, R. Viskanta, and M.Y. Chen, Effect of foam properties on heat transfer in high temperature open-cell foam inserts, *J. Am. Ceram. Soc.*, 95(2012), No. 6, p. 2015.
- [12] S.Y. Liu and H.M. Yang, Stearic acid hybridizing coal-series kaolin composite phase change material for thermal energy storage, *Appl. Clay Sci.*, 101(2014), p. 277.
- [13] Y. He, X. Zhang, and Y.J. Zhang, Preparation technology of phase change perlite and performance research of phase change and temperature control mortar, *Energy Build.*, 85(2014), p. 506.
- [14] H.L. Zhang, J. Baeyens, G. Cáceres, J. Degrève, and Y.Q. Lv, Thermal energy storage: Recent developments and practical aspects, *Prog. Energy Combust. Sci.*, 53(2016), p. 1.
- [15] Y.H. Chen, L.M. Jiang, Y. Fang, *et al.*, Preparation and thermal energy storage properties of erythritol/polyaniline form-stable phase change material, *Sol. Energy Mater. Sol. Cells*, 200(2019), art. No. 109989.
- [16] J.L. Zeng, Y.H. Chen, L. Shu, *et al.*, Preparation and thermal

- properties of exfoliated graphite/erythritol/mannitol eutectic composite as form-stable phase change material for thermal energy storage, *Sol. Energy Mater. Sol. Cells*, 178(2018), p. 84.
- [17] G.Y. Fang, H. Li, L. Cao, and F. Shan, Preparation and thermal properties of form-stable palmitic acid/active aluminum oxide composites as phase change materials for latent heat storage, *Mater. Chem. Phys.*, 137(2012), No. 2, p. 558.
- [18] X. Jin, M.A. Medina, and X.S. Zhang, On the importance of the location of PCMs in building walls for enhanced thermal performance, *Appl. Energy*, 106(2013), p. 72.
- [19] A. Sari and A. Biçer, Preparation and thermal energy storage properties of building material-based composites as novel form-stable PCMs, *Energy Build.*, 51(2012), p. 73.
- [20] D. Zhou, C.Y. Zhao, and Y. Tian, Review on thermal energy storage with phase change materials (PCMs) in building applications, *Appl. Energy*, 92(2012), p. 593.
- [21] Y. Zhou, S.C. Wang, J.Q. Peng, et al., Liquid thermo-responsive smart window derived from hydrogel, *Joule*, 4(2020), No. 11, p. 2458.
- [22] C.C. Li, J. Ouyang, and H.M. Yang, Novel sensible thermal storage material from natural minerals, *Phys. Chem. Miner.*, 40(2013), No. 9, p. 681.
- [23] D. Feldman, D. Banu, and D. Hawes, Low chain esters of stearic acid as phase change materials for thermal energy storage in buildings, *Sol. Energy Mater. Sol. Cells*, 36(1995), No. 3, p. 311.
- [24] B.S. Xie, C.C. Li, B. Zhang, L.X. Yang, G.Y. Xiao, and J. Chen, Evaluation of stearic acid/coconut shell charcoal composite phase change thermal energy storage materials for tankless solar water heater, *Energy Built Environ.*, 1(2020), No. 2, p. 187.
- [25] D.Y. Zhang, C.C. Li, N.Z. Lin, B.S. Xie, and J. Chen, Mica-stabilized polyethylene glycol composite phase change materials for thermal energy storage, *Int. J. Miner. Metall. Mater.*, 29(2022), No. 1, p. 168.
- [26] A. Arteconi, N.J. Hewitt, and F. Polonara, State of the art of thermal storage for demand-side management, *Appl. Energy*, 93(2012), p. 371.
- [27] B.M. Li, D. Shu, R.F. Wang, et al., Polyethylene glycol/silica (PEG@SiO<sub>2</sub>) composite inspired by the synthesis of mesoporous materials as shape-stabilized phase change material for energy storage, *Renewable Energy*, 145(2020), p. 84.
- [28] K.R. Arun, M. Srinivas, C.A. Saleel, and S. Jayaraj, Influence of the location of discrete macro-encapsulated thermal energy storage on the performance of a double pass solar plate collector system, *Renewable Energy*, 146(2020), p. 675.
- [29] X. Zeng, F. Wang, H.F. Zhang, L.J. Cui, J. Yu, and G.W. Xu, Extraction of vanadium from stone coal by roasting in a fluidized bed reactor, *Fuel*, 142(2015), p. 180.
- [30] C.C. Li, B.S. Xie, J. Chen, Z.X. He, Z.S. Chen, and Y. Long, Emerging mineral-coupled composite phase change materials for thermal energy storage, *Energy Convers. Manag.*, 183(2019), p. 633.
- [31] D. Yang, F. Peng, H.R. Zhang, et al., Preparation of palygorskite paraffin nanocomposite suitable for thermal energy storage, *Appl. Clay Sci.*, 126(2016), p. 190.
- [32] X.G. Zhang, R.L. Wen, Z.H. Huang, et al., Enhancement of thermal conductivity by the introduction of carbon nanotubes as a filler in paraffin/expanded perlite form-stable phase-change materials, *Energy Build.*, 149(2017), p. 463.
- [33] A.H. Alkhezaleh, Preparation and characterization of isopropyl palmitate/expanded perlite and isopropyl palmitate/nanoclay composites as form-stable thermal energy storage materials for buildings, *J. Energy Storage*, 32(2020), art. No. 101679.
- [34] C.C. Li, M.F. Wang, B.S. Xie, H. Ma, and J. Chen, Enhanced properties of diatomite-based composite phase change materials for thermal energy storage, *Renewable Energy*, 147(2020), p. 265.
- [35] W.T. Zhou, Y.X. Han, Y.S. Sun, and Y.J. Li, Strengthening iron enrichment and dephosphorization of high-phosphorus oolitic hematite using high-temperature pretreatment, *Int. J. Miner. Metall. Mater.*, 27(2020), No. 4, p. 443.
- [36] M. Diaz-Somoano and M.R. Martinez-Tarazona, Retention of arsenic and selenium compounds using limestone in a coal gasification flue gas, *Environ. Sci. Technol.*, 38(2004), No. 3, p. 899.
- [37] C.C. Li, H. Ma, B.S. Xie, et al., A comparison of mineralogical and thermal storage characteristics for two types of stone coal, *Minerals*, 9(2019), No. 10, art. No. 594.
- [38] R.L. Wen, X.G. Zhang, Z.H. Huang, et al., Preparation and thermal properties of fatty acid/diatomite form-stable composite phase change material for thermal energy storage, *Sol. Energy Mater. Sol. Cells*, 178(2018), p. 273.
- [39] D.S. He, Y. Chen, P. Xiang, Z.J. Yu, and J.H. Potgieter, Study on the pre-treatment of oxidized zinc ore prior to flotation, *Int. J. Miner. Metall. Mater.*, 25(2018), No. 2, p. 117.
- [40] C.C. Li, B. Zhang, and Q.X. Liu, N-eicosane/expanded graphite as composite phase change materials for electro-driven thermal energy storage, *J. Energy Storage*, 29(2020), art. No. 101339.
- [41] B.S. Xie, C.C. Li, and Y.L. He, Advanced electro-heat conversion properties of microcrystalline graphite-based composite phase change material with the three-dimensional framework, *J. Energy Storage*, 59(2023), art. No. 106367.
- [42] J. Liu, Y.M. Zhang, J. Huang, T. Liu, Y.Z. Yuan, and X.B. Huang, Influence of mechanical activation on mineral properties and process of acid leaching from stone coal, *Chin. J. Rare Met.*, 38(2014), No. 1, p. 115.
- [43] G.Y. Fang, H. Li, Z. Chen, and X. Liu, Preparation and characterization of stearic acid/expanded graphite composites as thermal energy storage materials, *Energy*, 35(2010), No. 12, p. 4622.
- [44] Y.P. Yuan, T.Y. Li, N. Zhang, X.L. Cao, and X.J. Yang, Investigation on thermal properties of capric-palmitic-stearic acid/activated carbon composite phase change materials for high-temperature cooling application, *J. Therm. Anal. Calorim.*, 124(2016), No. 2, p. 881.
- [45] C.C. Li, B.S. Xie, D.L. Chen, et al., Ultrathin graphite sheets stabilized stearic acid as a composite phase change material for thermal energy storage, *Energy*, 166(2019), p. 246.
- [46] C.C. Li, B. Zhang, B.S. Xie, et al., Stearic acid/expanded graphite as a composite phase change thermal energy storage material for tankless solar water heater, *Sustain. Cities Soc.*, 44(2019), p. 458.
- [47] A. Sari and A. Biçer, Thermal energy storage properties and thermal reliability of some fatty acid esters/building material composites as novel form-stable PCMs, *Sol. Energy Mater. Sol. Cells*, 101(2012), p. 114.
- [48] A. Sari, A. Karaipekli, and C. Alkan, Preparation, characterization and thermal properties of lauric acid/expanded perlite as novel form-stable composite phase change material, *Chem. Eng. J.*, 155(2009), No. 3, p. 899.
- [49] Z.M. Sun, Y.Z. Zhang, S.L. Zheng, Y. Park, and R.L. Frost, Preparation and thermal energy storage properties of paraffin/calcined diatomite composites as form-stable phase change materials, *Thermochim. Acta*, 558(2013), p. 16.
- [50] A. Sari and A. Karaipekli, Preparation, thermal properties and thermal reliability of capric acid/expanded perlite composite for thermal energy storage, *Mater. Chem. Phys.*, 109(2008), No. 2-3, p. 459.